JPE 16-1-12

http://dx.doi.org/10.6113/JPE.2016.16.1.102
ISSN(Print): 1598-2092 / ISSN(Online): 2093-4718

Contactless Power Charger for Light Electric Vehicles Featuring Active Load Matching

Wei Jiang†, Song Xu*, and Nailu Li*

†,*Department of Electrical Engineering, Yangzhou University, Yangzhou, China

Abstract

Contactless power transfer technology is gaining increasing attention in city transportation applications because of its high mobility and flexibility in charging and its commensurate power level with conductive power transfer method. In this study, an inductively coupled contactless charging system for a 48 V light electric vehicle is proposed. Although this study does not focus on system efficiency, the generic problems in an inductively coupled contactless power transfer system without ferromagnetic structure are discussed. An active load matching method is also proposed to control the power transfer on the receiving side through a load matching converter. Small signal modeling and linear control technology are applied to the load matching converter for port voltage regulation, which effectively controls the power flow into the load. A prototype is built, and experiments are conducted to reveal the intrinsic characteristics of a series–series resonant inductive power charger in terms of frequency, air gap length, power flow control, coil misalignment, and efficiency issues.

Key words: Contactless power transfer, Electric vehicle, Load matching

I. INTRODUCTION

Unlike fast-developing, highly penetrated, and high-mobility information technology, power transmission systems still rely on conductive energy transfer. Extensive designs with contactless power transfer (CPT) systems [1], including industrial conveyance systems and vehicle battery-charging systems, exist, and their system efficiency reaches up to 90% [2]-[8].

The air gap length in inductively coupled CPT applications has been restricted to the close proximity range in contrast to transmitter/receiver coil size. References [5]-[7] proposed inductive CPT applications from low power electronics to heavy industry. References [8]-[11] evaluated the inductive CPT in low-voltage (LV) applications, such as electric vehicles (EVs), in terms of cost, efficiency, and converter topologies. In the aforementioned applications, the converter switching frequency is limited below hundreds of kilohertz for loss control purpose. Ferrite structures are widely used in the literature to facilitate energy transfer and to protect against magnetic flux irradiation [2]-[13]. Reference [12] studied the alignment issues in inductively coupled CPT application by passively compensating for leakage inductance. Reference [13] eliminated misalignment problems through a carefully designed guide rail structure.

Strongly coupled magnetic resonance offers omnidirectional transmission distance that is longer than that of the inductively coupled CPT [4]. Given that the coil quality factor dominates the spatial energy transfer, the coil design and associated passive components selection becomes crucial for such CPT system. References [14]-[22] discussed the properties and performance improvement of such systems through detailed modeling, frequency optimization, coil design, and impedance matching. However, high-efficiency power electronic converters that operate in the megahertz range remain a great challenge for magnetic resonance CPT applications.

Inductive coupled and magnetic resonance CPT technologies and microwave and electric field coupling methods are also discussed in the literature for specialized applications [23], [24].

Conventional isolated sensing methods, such as Hall effect and opto-coupling, are impractical because of spatial separation between the sending and the receiving coils. The load feedback control of a CPT can be implemented through several ways. References [25]-[27] used active bridge topology at both sides. Both primary side and secondary side

Manuscript received Mar. 20, 2015; accepted Aug. 16, 2015
Recommended for publication by Associate Editor Hao Ma.
†Corresponding Author: jiangwei@yzu.edu.cn
Tel/Fax: +86-051487971315, Yangzhou University
*Department of Electrical Engineering, Yangzhou University, China

regulations were implemented by applying phase shift control, in which a well-designed phase lock loop is essential for power control. References [28] and [29] applied the frequency modulation method to regulate load power. The load power information is fed back via a wireless communication channel from the receiving side. Reference [29] also proposed a charger controller for load power regulation through load current feedback. Reference [30] proposed a chopper circuit to modulate the load to control the power flow, in which the chopper switching period and the resonant frequency was matched precisely for the load power transfer.

Electric propulsion is becoming increasingly popular in city transportation systems. Although high-power applications, such as electric city buses and electric cars, are still not prevalent, medium-low power level applications, such as electric bikes, are well developed and affordable. E-bikes are usually equipped with a 36 or 48V lead–acid battery pack with a brushless DC motor as the driving unit. A series-excited brushed DC motor supplied with a 48 or 72V battery pack is more popular in medium power vehicles, such as service vehicles and electric forklifts. Contactless charger offers an automatic charging solution to the large number of EVs, which are considered a possible candidate for the imminent city transportation infrastructure.

An inductively coupled contactless power charger for a 48V EV is proposed in this study. The main power stages of the systems, including a high-frequency inverter, resonant network without ferrite, full-bridge rectifier, and load matching converter, are evaluated and designed. Although this study does not focus on system efficiency, an active load matching method is proposed to control the contactless power flow on the receiving side. The prototype is built with a digital signal controller (DSC) as the control unit. Tests are performed to quantify and reveal the intrinsic characteristics of a series–series resonant inductive power charger in terms of frequency, air gap length, power flow control, coil misalignment, and efficiency issues.

II. CPT Charger System Structure

Charging infrastructures in cities are usually constructed beneath sheds. Thus, a solar power roof mount is considered the main input to the charger system. Therefore, the charger system is designed with an LV input. The proposed system structure, which consists of an inverter, resonant network, rectifier, and load matching converter, is illustrated in Fig. 1. A full-bridge inverter (FBI) is used to interface the LV DC input to utilize the LV input fully, as shown in Fig. 1(b). A medium-frequency square wave is obtained with the FBI to drive a sending-side series resonant network through L_1 and C_1. On the receiving side, the receiving coil L_2 and a series connected capacitor C_2 form the secondary resonant tank,

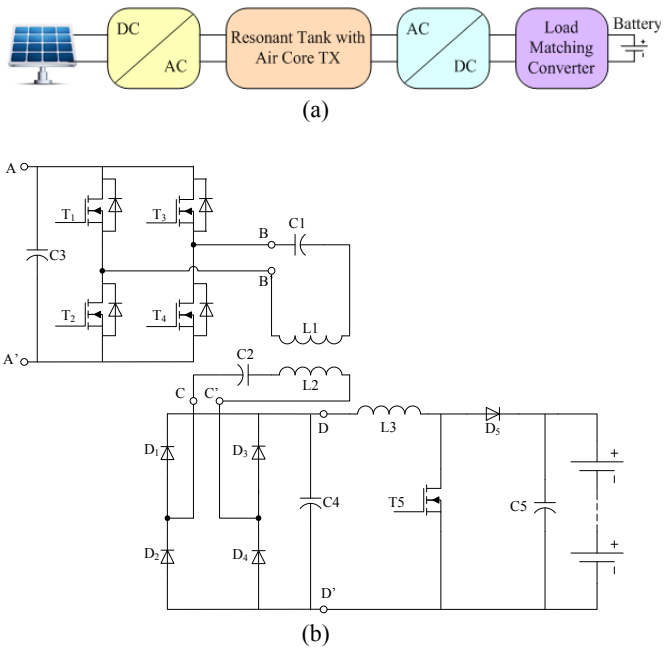

Fig. 1. Contactless power charger: (a) system structure and (b) circuit schematic.

which is connected to the AC terminal of a full-bridge rectifier with large output capacitance. A ferrite structure is not considered to achieve a compact design in a highly vibrational driving condition. An impedance matching converter, which is a boost converter in this case, is connected between the rectifier and battery load for charging power conditioning.

III. Analysis of Inductive Power Transfer

A. Analysis of Series Resonant Power Transfer

A conventional voltage-source square-wave inverter is chosen as the sending-end converter, such that the LV solar input can be fully utilized and transferred by the downstream resonant network. The series resonant structure is chosen over the parallel structure because of its good current limiting nature as a series-connected variable impedance, where the resonance frequency f_r is given by

$$f_r = \frac{1}{2\pi\sqrt{L_1 C_1}} = \frac{1}{2\pi\sqrt{L_2 C_2}} \quad (1)$$

where $L_{1,2}$ and $C_{1,2}$ are the series capacitance and coil inductance (including leakage), respectively.

The series–series (SS) resonant topology is shown in Fig. 2, where the self-inductance from the sending and receiving coils is analyzed in a T-equivalent circuit. M is the mutual inductance, whereas R_1 and R_2 are the equivalent series resistance (ESR) for the coil and resonant capacitor. A simple AC circuit analysis is performed, and the ideal efficiency can be obtained as in Equ. (2) through the relationship between the primary current I_1 and secondary current I_2 in condition (3).

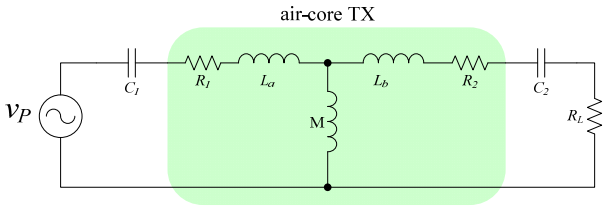

Fig. 2. SS resonant topology.

As can be observed in the expression, the energy transfer efficiency is closely related to the coupling factor and the quality factor of the resonant network. The maximum efficiency can be obtained by Equ. (4) if the squares of operation frequency is sufficiently larger than the term $R_1 \cdot (R_L+R_2)/M^2$.

$$\eta = \frac{I_2^2 R_L}{I_p^2 R_1 + I_s^2 R_2 + I_2^2 R_L} = \frac{R_L}{(R_L + R_2)\left[1 + \frac{R_1 (R_L + R_2)}{\omega_r^2 M^2}\right]} \tag{2}$$

$$\frac{I_1}{I_2} = \frac{R_2 + R_L}{\omega_0 M} \tag{3}$$

$$\eta_{MAX} = \frac{R_L}{R_2 + R_L} \tag{4}$$

The maximum efficiency in the reduced expression (4) depends on the receiving side parasitic parameters and load. Load resistance is usually considerably larger than the secondary parasitic resistance. Thus, the maximum theoretical efficiency is high. We can also infer that load variation does not substantially affect the efficiency in a medium-low CPT system.

B. Load Matching Converter Design

As a DC–DC converter with continuous input power, the boost converter is particularly useful in load-shaping applications, such as photovoltaic power conditioning and power factor correction. In these applications, the boost converter, as an active load, can change the steady-state impedance, such that the source can detect different loads during the power transfer.

As discussed, the power control function is required in a battery charger application. Thus, the concept of loss-free resistor is adopted, as indicated in Fig. 3. This resistor is a boost converter with S_1 and S_2 switching synchronously. The boost converter can shape the port variable such that the port impedance can be adjusted to the desired value. The power flow into the battery can be controlled properly by adjusting the impedance of the load matching converter.

As an SS resonant topology is inherently a current link topology in a small-signal sense. The uncontrolled rectifier with a large output capacitor is used as a voltage sink to interface the current link topology. The rectifier shows voltage source characteristics to the downstream converter because of the large output capacitance. Therefore, regulating the port voltage v_1 in Fig. 3 with a current–sink circuit helps

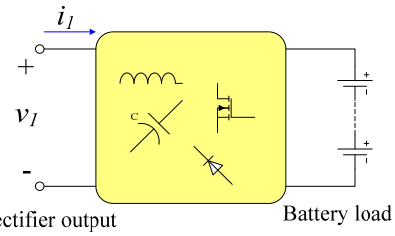

Fig. 3. Load matching with a power converter.

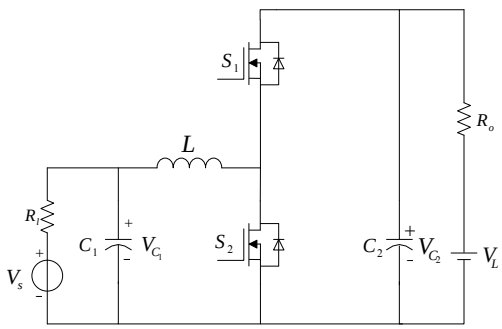

Fig. 4. Schematic of a load-matching converter.

regulate the power transferred from the sending end. Unlike the control methods in [28] and [30], port voltage is a direct state variable to the boost converter circuit, which can be adjusted continuously without jeopardizing the trajectories of the other state variables, particularly the inductor L current.

The average switch model is used to obtain the transfer function of the load-matching converter. The input resistance R_i is obtained by the rated power of 200 W, and R_o is the battery ESR at 80% state of charge. The transfer function of the duty cycle to the input voltage is determined by applying small signal perturbations, as in Equ. (5). This transfer function is a third-order system with a zero on the numerator. The negative sign indicates that the input voltage decreases with the positive perturbation of the duty cycle, which can be ensured by flipping the control logic in the feedback loop.

$$G_{Vc1d} = -\frac{as + b}{cs^3 + ds^2 + es + f} \tag{5}$$

in which

$$\begin{aligned} a &= R_i R_o V_{C2} C_2 \\ b &= R_i R_o I_L (1-D) + R_s V_{C2} \\ c &= R_i R_o C_1 C_2 L \\ d &= R_i C_1 + R_o C_2 \\ e &= R_i R_o [(1-D)^2 C_1 + C_2] + L \\ f &= R_l + (1-D)^2 R_o \end{aligned}$$

$$C_V(s) = k \frac{(1 + \frac{s}{\omega_z})}{1 + \frac{s}{\omega_p}} \tag{6}$$

A double-pole single-zero PI controller is proposed, as in Equ. (6). The position of the feedback and the reference is

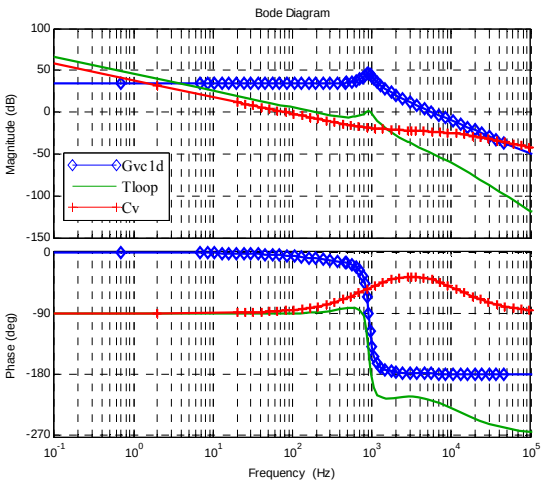

Fig. 5. Bode plot for port voltage regulation loop.

flipped in the digital implementation because of the negative sign in the G_{vc1d}. Hence, this position is neglected in the loop analysis. The bode plot for the compensated system open loop transfer function T_{loop}, plant G_{vc1d}, and voltage controller C_v is plotted, as illustrated in Fig. 5. Given that the charging occurs during the parking state, no dynamic misalignment or air gap variation is assumed. Therefore, the power to be transferred to the battery is not necessarily regulated tightly. Based on this criterion, the load matching controller is designed conservatively, thereby resulting in a cross-over frequency of 2 Hz and a phase margin of 91.5°, as indicated in Fig. 5.

IV. Experiment Results and Analysis

A. Prototype Setup and Frequency Test

The hardware prototype is implemented, and a 16-bit dsPIC controller with a 40 MHz clock is used as the controller. An adjustable bench power supply with 30 V and 20 A is selected as the input source to prove the principle. The load is a lead–acid battery pack rated at 48 V and 100 Ah. The major system parameters are listed in Table I.

Fig. 6 shows the prototype and the test bed. The experiments are conducted under different scenarios.

Frequency sweep and transient test are performed first to ensure the frequency characteristics and the feasibility of the hardware design. Fig. 7 shows the start-up transient of 200 W power transfer when the full-bridge converter works at 32 kHz. The waveform indicates that the system can achieve smoothed output power transfer without oscillated voltage or current in the steady state. The resonant inverter is designed to achieve a stable operation on the circuit level by operating at the slightly inductive region. Fig. 8 shows the phase delay between the inverter output voltage and current waveform on the sending end. The coil current lags slightly behind the inverter voltage, which is suitable for series resonant operation.

TABLE I
SYSTEM PARAMETERS

Component/ operation condition	Value
L_1	26 uH
C_1	0.98 uF
L_2	28.5 uH
C_2	0.88 uF
f_s	31.5 kHz
f_{pwm}	50 kHz
T_s	100 us
Air gap	33–72 mm
Coil size	170 mm × 250 mm

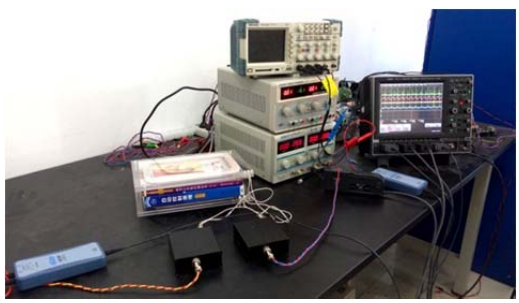

Fig. 6. Hardware prototype and test bed.

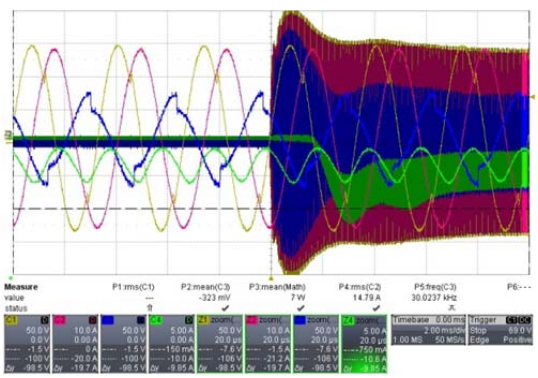

Fig. 7. Startup transient under an open-loop load-matching control.

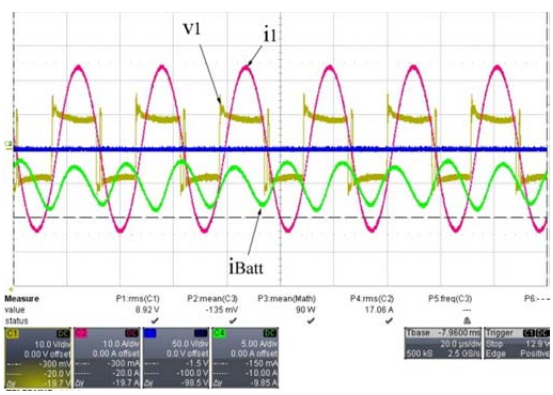

Fig. 8. Steady-state performance at tuned frequency; v1 - inverter output voltage (10V/div), i1 - sending coil current (10A/div), iBatt - battery charging current (5 A/div).

B. Active Load Matching Test and Analysis

The active load matching is verified by fixing the system input voltage and by varying the load-matching converter input voltage control reference V_{dc}^{*}. The air gap length is set at 70 mm. The sending and receiving coil voltages v_1 and v_2, input source current i_s, and battery charging current i_{Batt} are measured at different rectifier output voltages v_{dc}, as shown in Fig. 9. The voltage glitch across the coil reflects the inverter output voltage, which is experimentally verified with KVL. Figs. 9(a) to 9(e) illustrate that the rectifier output voltage v_{dc} is regulated to different levels from 13 V to 21 V, respectively. As v_{dc} increases, both input current and charging current increase; the charging power also increases. The effective charging power control via the proposed active load matching method is demonstrated.

Fig. 10 shows the collective experimental results with active load matching control at three different air gap lengths; these results indicate the susceptibility of the transferred power to the port voltage v_{dc}. Both input and output powers increase linearly with the load port voltage v_{dc} in Fig. 10(a), while the system efficiency remains nearly constant during the load match for different power levels. Thus, the conclusions in Section III A are confirmed.

C. Sensitivity Analysis

A series of sensitivity tests is performed. As confirmed in Section IIIA, load port voltage dominates the transferred power. The influences from air gap and coil misalignment are studied in the following test. The charging power is maintained at 200 W to ensure fair comparisons.

The coil size is relatively compact for a light EV (e-bike), which is only 170 mm × 250 mm. No high magnetic permeability structure exists at either side to assist the coupling. Therefore, the designed maximum air gap length is within the half short side length of the coil. In the air gap sensitivity test, the air gap length is swept from 30 mm to 75 mm. As can be observed from the data in Fig. 11, the efficiency drops as the air gap increases. Distance plays an important role in an inductively coupled CPT because the power transfer is closely related to the linkage between the two coils. The test results also indicate that the maximum air gap length can be increased if the sending/receiving coil size is increased.

The misalignment tests are carried out under horizontal and vertical misalignment conditions. As indicated in Fig. 12, both Δd and Δl are swept from 0 to 70 mm. The maximum misalignment is also visually noticeable to vehicle drivers during vehicle parking and can be corrected by the driver easily.

Fig. 13 shows the misalignment test results under different air gap lengths. The output power is fixed at 200 W in the tests. Horizontal misalignment tests indicate approximately 10% efficiency drop throughout the

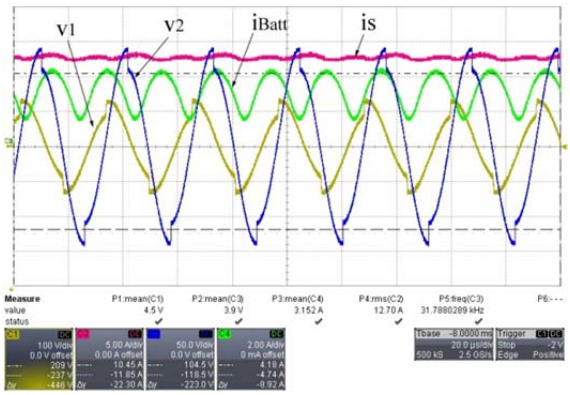

(a)

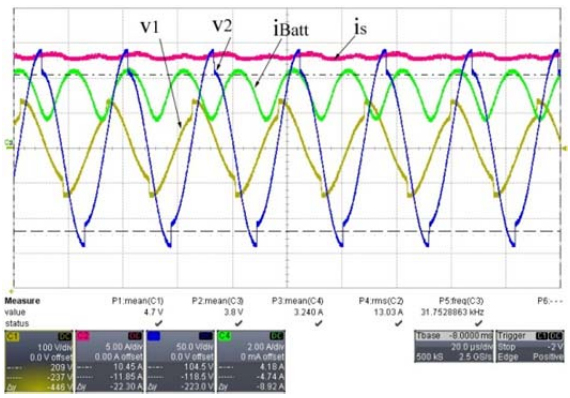

(b)

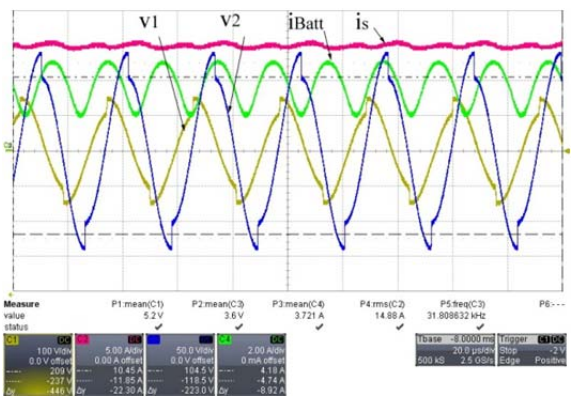

(c)

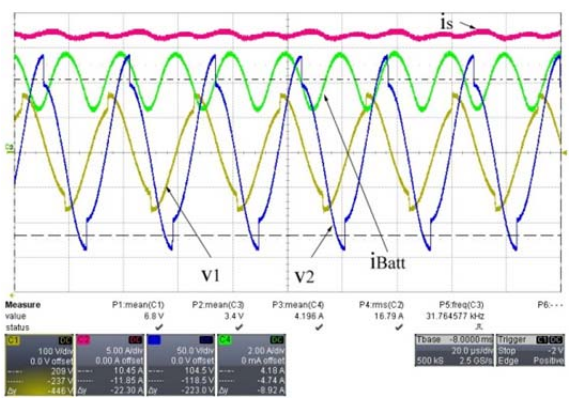

(d)

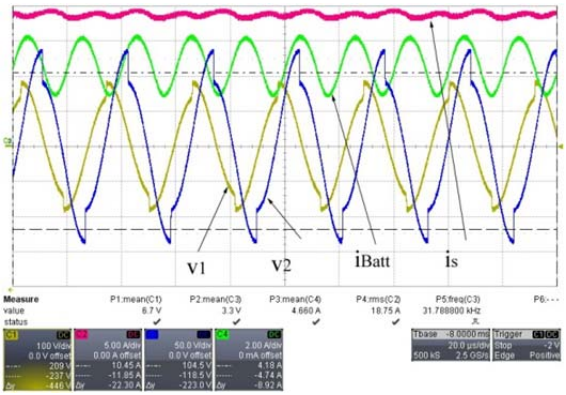

(e)

Fig. 9. Active load matching control with variable rectifier output voltage, 2 us/div; is - dc input current (5A/div); iBatt - battery charging current (2A/div); v1 - sending coil voltage (100 V/div); v2 - receiving coil voltage (50 V/div): (a) vdc = 13 V, (b) vdc = 14 V, (c) vdc = 16 V, (d) vdc = 19 V, and (e) vdc = 21 V.

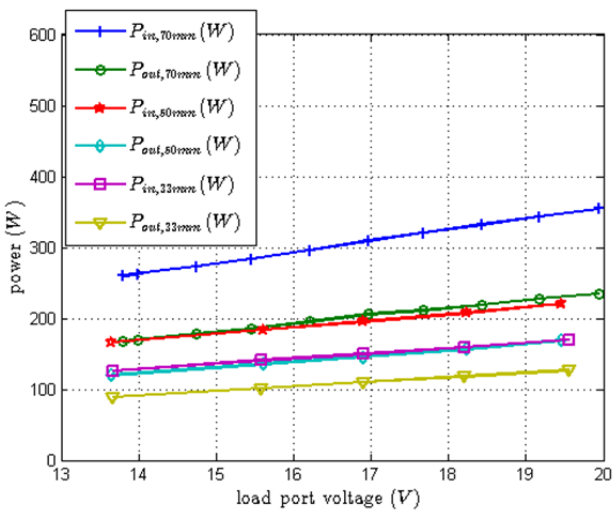

(a)

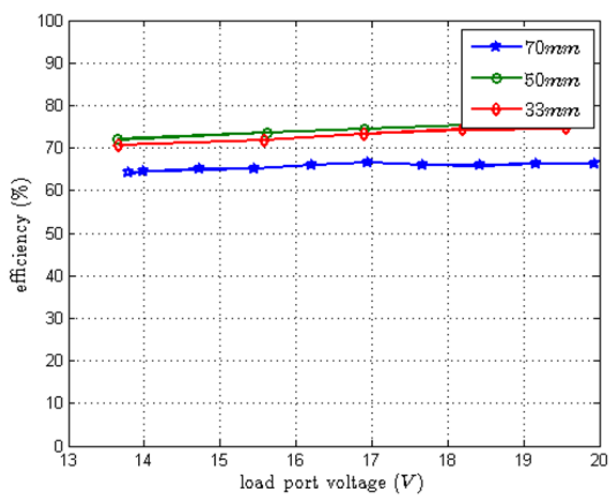

(b)

Fig. 10. CPT via active load matching at different air gap lengths: (a) input and output powers and (b) system throughout efficiency.

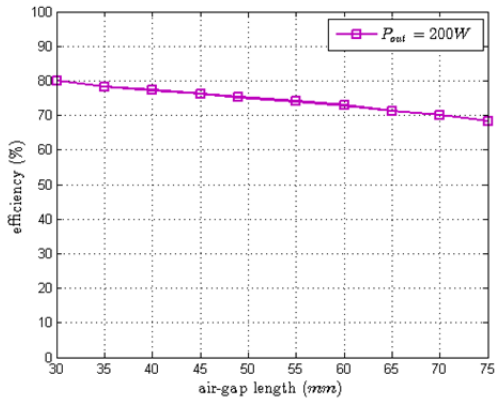

Fig. 11. System efficiency at 200 W output power with different air gap distances.

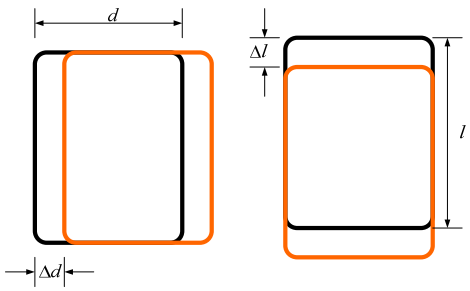

Fig. 12. Horizontal and vertical misalignment condition setup.

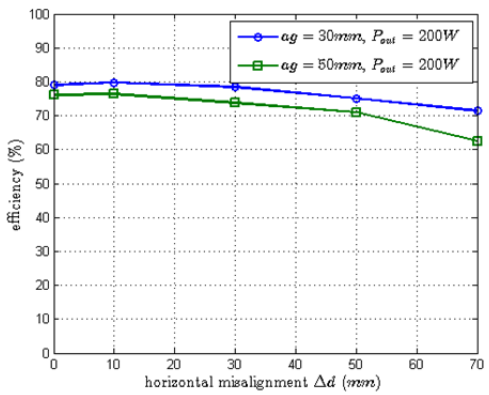

(a)

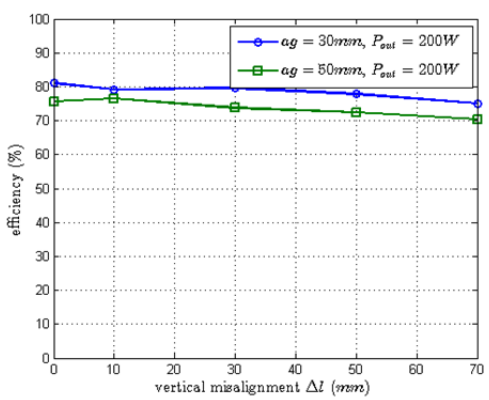

(b)

Fig. 13. Efficiency measurement with coil misalignment: (a) horizontal misalignment and (b) vertical misalignment.

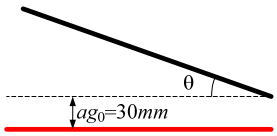

Fig. 14. Tilting condition setup.

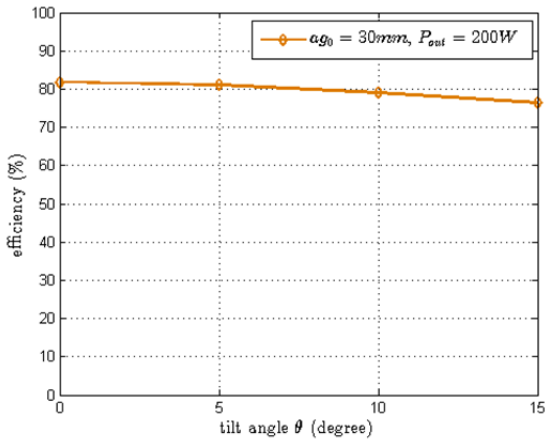

Fig. 15. Efficiency variation with tilting angle.

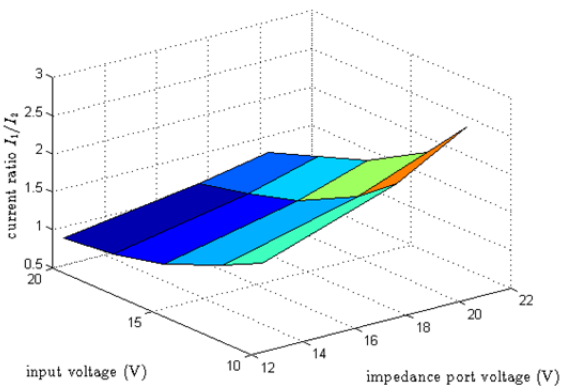

Fig. 16. Current transfer ratio plot at 70 mm air gap.

misalignment range, whereas only a 5% drop exists in the vertical misalignment conditions.

The tilting angles between the sending and receiving coils vary under the full alignment condition, as shown in Fig. 14. The efficiency under 200 W load power condition undergoes a 6% drop when the tilting angle changes from 0 to 15 degrees.

The misalignment at different directions reflects changes in the coil overlapping area. Thus, the power transfer efficiency is affected by the effective coil overlapping area. The performance of the charger stays within an acceptable range.

The measurement of the sending and receiving coil voltages in Fig. 9 does not reflect a clear relationship between these two voltages because of the voltage deformation caused by power electronic circuits. Therefore, tests are performed to investigate the coupling by varying both input source voltage and load matching port voltage. The coil current is sinusoidal in the resonant state. Thus, a comparison between the sending coil current I_1 and receiving coil current I_2 is performed. The relationship among the current transfer ration I_1/I_2, input source voltage, and load matching port voltage is obtained in Fig. 16. The "coupling" k is typically used in analyzing the inductive coupled CPT. Thus, the data obtained from the experimental work does not show explicit coupling behavior by observing the current transfer ratio. This result is due to an extra current shunt path formed by the mutual inductance M in the canonical T-model, which is not negligible compared with a traditional power transformer. Therefore, applying linear magnetic circuit analysis in static performance prediction in a CPT system with power electronic conditioners is challenging. However, the flow of power can be controlled in a close loop, which renders predictable power transfer behaviors, through the proposed active load matching method.

V. Conclusion

An inductive coupled contactless charger for a 48 V light EV is proposed in this paper. The main power stages of the system, including the high-frequency inverter, resonant network, full-bridge rectifier, and load matching converter (the boost converter), are evaluated and designed. Although this study does not focus on the system efficiency, an active load matching method is proposed to control CPT. The prototype is built with a dsPIC DSC. The tests are conducted in several meaningful scenarios to illustrate the multifold characteristics of the proposed contactless power charger without ferrite structure support. Experimental verification includes the frequency characteristics of SS resonant topology, the sensitivity of some important system parameters, and the power flow control method. On the basis of the experimental results, the following conclusions can be obtained:

- The efficiency remains nearly constant for a wide range of charging power levels, and efficiency increases when the air gap length decreases.
- The performance of the charger stays within an acceptable range in case of coil misalignment.
- The proposed active load matching method can avoid uncertainties in power coupling and effectively regulate the transferred power in a controllable manner.

Acknowledgment

This work is sponsored by the National Natural Science Foundation of China (grant number 51207135), Jiangsu Natural Science Foundation (grant number BK2012266), and YZU-Yangzhou City Joint Fund (grant number 2012038-10), CSC No. 201409300007.

References

[1] G. A. Covic and J. T. Boys, "Inductive power transfer,"

Proceedings of the IEEE, Vol. 101, No. 6, pp. 1276-1289, Jun. 2013.

[2] M. Budhia, G. A. Covic and J. T. Boys, "Design and optimization of circular magnetic structures for lumped inductive power transfer systems," *IEEE Trans. Power Electron*., Vol. 26, No. 11, pp. 3096-3108, Nov. 2011.

[3] C. Wang, G. A. Covic and O. H. Stielau, "Power transfer capability and bifurcation phenomena of loosely coupled inductive power transfer systems," *IEEE Trans. Ind. Electron.*, Vol. 51, No. 1, pp. 148-157, Feb. 2004.

[4] H. L. Li, A. P. Hu, and G. A. Covic, "Primary current generation for a contactless power transfer system using free oscillation and energy injection control," *Journal of Power Electronics*, Vol. 11, No. 3, pp.256-263, May 2011.

[5] Y. Jang and M. M. Jovanovic. "A contactless electrical energy transmission system for portable-telephone battery chargers," *IEEE Trans. Ind. Electron*., Vol. 50. No. 3, pp. 520-527, Jun 2003.

[6] K. W. Klontz, D. M. Divan, D. W. Novotny, and R. D. Lorenz, "Contactless power delivery system for mining applications," *IEEE Trans. Ind. Appl*., Vol. 31, No. 1, pp. 27-35, Jan./Feb. 1995.

[7] M. L. G. Kissin, H. Hao, and G. A. Covic, "A practical multiphase IPT system for AGV and roadway applications," in *IEEE Energy Conversion Congress and Exposition(ECCE)*, pp. 1844–1850, Sep. 2010.

[8] M. A. Bloom, N. Geng, and M. Krishnamurthy, "Design considerations for wireless electric vehicle charging," in *IEEE Transportation Electrification Conference and Expo(ITEC)*, pp.1-6, Jun. 2013.

[9] S. Jeong, Y. J. Jang, and D. Kum, "Economic analysis of the dynamic charging electric vehicle," *IEEE Trans. Power Electron.*, Vol. 30, No. 11, pp. 6368-6377, Nov. 2015.

[10] B. Esteban, M. Sid-Ahmed, and N. C. Kar, "A comparative study of power supply architectures in wireless EV charging systems," *IEEE Trans. Power Electron*., Vol. 30, No. 11, pp. 6408-6422, Nov. 2015.

[11] H. R. Rahnamaee, D.J. Thrimawithana, and U.K. Madawala, "MOSFET based Multilevel converter for IPT systems," in *IEEE International Conference on Industrial Technology(ICIT)*, pp. 295-300, Feb./Mar. 2014.

[12] D. Kumrschner, C. Rathge, and U. Jumar, "Design methodology for high efficient inductive power transfer systems with high coil positioning flexibility," *IEEE Trans. Ind. Electron*., Vol. 60, No. 1, pp. 372-381, Jan. 2013.

[13] H. Z. Z. Beh, G. A. Covic, and J. T. Boys, "Wireless fleet charging system for electric bicycles," *IEEE Journal of Emerging and Selected Topics in Power Electronics*, Vol. 3. No. 1, pp. 75-86, Mar. 2015.

[14] A. Kurs, A. Karalis, R. Moffatt, J. D. Joannopoulos, P. Fisher, M. Soljačić, "Wireless power transfer via strongly coupled magnetic resonances," in *Science Express on 7* Vol. 317, No. 5834, pp. 83–86, Jun. 2007.

[15] C.-J. Chen, T.-H. Chu, C.-L. Lin, and Z.-C. Jou, "A study of loosely coupled coils for wireless power transfer," *IEEE Trans. Circuits Syst. II, Exp. Briefs*, Vol. 57, No. 7, pp. 536-540, Jul. 2010.

[16] J. Huh, W. Lee, S. Choi, G. Cho, and C. Rim, "Frequency-domain circuit model and analysis of coupled magnetic resonance systems," *Journal of Power Electronics*, Vol. 13, No. 2, pp.275-286 , Mar. 2013.

[17] T. C. Beh, T. Imura, M. Kato, and Y. Hori, "Basic study of improving efficiency of wireless power transfer via magnetic resonance coupling based on impedance matching," in *IEEE International Symposium on Industrial Electronics(ISIE)*, pp. 2011-2016, Jul. 2010.

[18] Y. Li, Q. Yang, H. Chen, X. Zhang, and Z. Yan, "Experimental system design of wireless power transfer based on witricity technology," in *International Conference on Control, Automation and Systems Engineering(CASE)*, pp. 1-3, Jul. 2011.

[19] X. Zhang, S. L. Ho, and W. N. Fu, "Quantitative analysis of a wireless power transfer cell with planar spiral structures," *IEEE Trans. Magn*., Vol. 47, No. 10, pp. 3200-3203, Oct. 2011.

[20] D. G. Nottiani and F. Leccese, "A simple method for calculating lumped parameters of planar spiral coil for wireless energy transfer," in *11th International Conference on Environment and Electrical Engineering(EEEIC)*, pp. 869–872, 2012.

[21] A. E. Gundogdu and E. Afacan, "The effect of frequency, multi resonator and relay resonator conditions on wireless power transmission," in *Wireless Telecommunications Symposium(WTS)*, pp. 1-5, 2012.

[22] V. Jiwariyavej, T. Imura, and Y. Hori, "Coupling coefficients estimation of wireless power transfer system via magnetic resonance coupling using information from either side of the system," *IEEE Journal of Emerging and Selected Topics in Power Electronics*, Vol. 3. No. 1, pp. 191-200, Mar. 2015.

[23] N. Shinohara, Y. Kubo, and H. Tonomura, "Wireless charging for electric vehicle with microwaves," in *3rd International Electric Drives Production Conference(EDPC)*, pp. 1-4, Oct. 2013.

[24] K. H. Yi, "6.78MHz capacitive coupling wireless power transfer system," *Journal of Power Electronics*, Vol. 15, No. 4, pp.987-993, Jul. 2015.

[25] U. K. Madawala and D. J. Thrimawithana, "A bidirectional inductive power interface for electric vehicles in V2G systems," *IEEE Trans. Ind. Electron*., Vol. 58. No. 10, pp. 4789-4796, Oct. 2011.

[26] U. K. Madawala, M. Neath, and D. J. Thrimawithana, "A power–frequency controller for bidirectional inductive power transfer systems," *IEEE Trans. Ind. Electron.*, Vol. 60, No. 1, pp. 310-317, Jan. 2013.

[27] T. Diekhans and R. W. De Doncker, "A dual-side controlled inductive power transfer system optimized for large coupling factor variations and partial load," *IEEE Trans. Power Electron*., Vol. 30, No. 11, pp. 6320-6328, Nov. 2015.

[28] R. Bosshard, J. W. Kolar, and B. Wunscht. "Control method for inductive power transfer with high partial-load efficiency and resonance tracking," in *International Power Electronics Conference*, pp. 2167-2174, May 2014.

[29] J. Hou, Q. Chen, S.-C. Wong, C. K. Tse, and X. Ruan, "Analysis and control of series/series-parallel compensated resonant converter for contactless power transfer," *IEEE Journal of Emerging and Selected Topics in Power Electronics*, Vol. 3. No. 1, pp. 124-136, Mar. 2015.

[30] D. Ahn and S. Hong. "Wireless power transfer resonance coupling amplification by load-modulation switching controller," *IEEE Trans. Ind. Electron*., Vol. 62. No. 2, pp. 898-909, Feb. 2015.

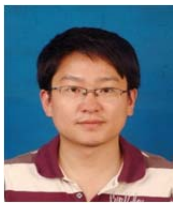

Wei Jiang was born in Yangzhou, China, in 1980. He received his B.S. degree from Southwest Jiaotong University, Chengdu, China, in 2003, and his M.Sc. and Ph.D. degrees in Electrical Engineering from the University of Texas at Arlington in Arlington, Texas, in 2006 and 2009, respectively. From 2007 to 2008, he worked at EF Technologies L.L.C. as a senior design engineer. In 2010, he joined Yangzhou University as a lecturer and founded the Smart Energy Laboratory, where he is the current associate professor. He is on sabbatical leave in the University of Strathclyde, Glasgow, UK, as a visiting professor. His current research interests include digitalized power conditioning to renewable energy and energy storage devices and microscopic analysis of electromechanical energy conversion.

Song Xu was born in China in 1992. He received his B.S. degree (first class with distinction) from the School of Energy and Power Engineering, Yangzhou University, Yangzhou, China, in 2014. He is currently working toward his M.Sc. degree in the same university. His research interests include contactless power transfer techniques and energy harvesting technologies.

Nailu Li graduated from the University of Wyoming, USA, in 2013. She is a member of the IEEE, AIAA, and AMSE. She is now an assistant professor in the School of Hydraulic, Energy, and Power Engineering at Yangzhou University, China. Her research areas mainly include adaptive control and stability theorem and monitoring wind power generation systems. She has been involved in several conference invited sessions, such as the 2012 ASME DSCC invited session, the 2012 AIAA GNC invited session, the 2013 AIAA AFM-ASE invited session, and the 2014 American Control Conference invited session.